Dalton Transactions

COMMUNICATION

View Article Online
View Journal | View Issue

Cite this: *Dalton Trans.*, 2018, **47**, 9226

Received 29th May 2018,
Accepted 16th June 2018

DOI: 10.1039/c8dt02196a

rsc.li/dalton

Small molecule activation with divalent samarium triflate: a synergistic effort to cleave O_2†

Mathieu Xémard,[a] Marie Cordier,[a] Elisa Louyriac,[b] Laurent Maron,[b] Carine Clavaguéra *[c] and Grégory Nocton *[a]

The divalent samarium triflate salt does not react with CO_2 or water, but does react with traces of O_2 or N_2O to form a tetrameric bis-oxo samarium motif. The reaction with O_2 is a $4e^-$ reductive cleavage where the electrons are coming from four different samarium centers. This highlights a rare synergistic effect for cleaving O_2, which has no precedent in divalent lanthanide complexes. Additionally, the addition of CO_2 to the tetrameric bis-oxo intermediate leads to the formation of a tetrameric bis-carbonate samarium triflate. Thus, the concomitant reaction of CO_2 with traces of O_2 leads to the same bis-carbonate tetrameric assembly.

The chemistry of low-valent coordination compounds has multiple advantages, of which small molecule activation is prominent because of the growing importance of transforming abundant molecules, such as N_2, H_2O and O_2,[1–6] and/or pollutant molecules, such as N_2O,[7] NO_x,[8] CO[9,10] and CO_2,[11] at low economical and environmental cost. In this context, electron rich transition metal complexes or low-valent uranium are often used since they allow multiple electron-transfer steps, leading to the complete reductive cleavage of the considered small molecule.[12–17]

On the other hand divalent lanthanides do not allow multiple electron transfers[4,6,18,19] as the trivalent form is the most stable one, except in the case of Ce^{III}, which is easily oxidized to formal Ce^{IV}.[5,6,20–24] However, once the single electron transfer step has occurred, the development of a radical on the small molecule often leads to further reactivity in terms of either radical-coupling reactions[25,26] or the formation of a dianionic species *via* the combination of the radical intermediate with a second coordination metal compound.[27] The synergy between two metallic fragments provides two electrons for the reduction of the substrate, and the reaction with N_2O forms oxo dimers,[7] while the reaction with CO_2 leads to oxalate or carbonate species depending on various factors.[11,28–30]

The mechanism of the carbonate formation is particularly interesting since it involves a bent CO_2^{2-} fragment formed in between two lanthanide metal centers, which further reacts with another CO_2 to yield CO and CO_3^{2-}.[31] The overall reaction is a two-electron disproportionation of CO_2 and has the important drawback of releasing CO, which is also a pollutant. In a recent report, we detailed the reaction of bulky samarium complexes with CO_2 to form carbonate species.[30] In this previous work, the use of low quality CO allowed for the serendipitous formation of a rare peroxo samarium dimer from the reaction with traces of oxygen.[30] In an opposite strategy to the typical one, in which the bulk increase allows for cleaner reactions *via* kinetic control, we reasoned that the decrease in the bulk of the ligand set on the samarium center would possibly allow for the involvement of more than two samarium centers, *i.e.* more than two electrons. The triflate ligand set is particularly interesting in this matter since it is a multidentate ligand[32] that usually facilitates the formation of large assemblies.[33]

The present work reports the reactivity studies of O_2, CO_2 and N_2O with a $Sm^{II}(OTf)_2(dme)_2$ complex and highlights the formation of two tetrametallic assemblies of Sm^{III}. The reductive cleavage of O_2 and the formation mechanism of a carbonate containing tetramer will be discussed.

The reaction of a deep purple solution of $Sm^{II}(OTf)_2(dme)_2$ in THF with one atmosphere of clean CO_2 does not lead to any discolouration, and there is no change in the ^{19}F NMR spectrum. This contrasts with the many other reports in the literature, including ours, which describe a fast reactivity of CO_2 with divalent samarium complexes at room temperature. However, the redox potential of samarium is known to be extremely dependent on the ligand.[34] Additionally, the addition of several equivalents of water does not modify the outcome of the reactions. However, when CO_2 of lower quality is used or when traces of O_2 are allowed in through the experi-

[a]*LCM, CNRS, Ecole polytechnique, Route de Saclay, 91128 Palaiseau Cedex, France. E-mail: greg.nocton@polytechnique.edu*
[b]*LPCNO, UMR 5215, Université de Toulouse-CNRS, INSA, UPS, Toulouse, France*
[c]*Laboratoire de Chimie Physique, CNRS-Université Paris-Sud, Université Paris-Saclay, 15 avenue Jean Perrin, 91405 Orsay Cedex, France. E-mail: carine.clavaguera@u-psud.fr*

†Electronic supplementary information (ESI) available: Details on synthesis, reactivity studies, ^{19}F NMR studies, theoretical calculations and X-ray studies. CCDC 1833702–1833705. For ESI and crystallographic data in CIF or other electronic format see DOI: 10.1039/c8dt02196a

mental protocol, the purple THF solution of $Sm^{II}(OTf)_2$ slowly fades until it becomes clear. After filtration of the solution, pentane layering allowed for the formation of transparent crystals that were analyzed as a tetrameric assembly of a samarium-containing two carbonate dianion, $[Sm_4(\mu_3\text{-}CO_3\text{-}\kappa_4O,O',O'')_2(\mu_2\text{-}OTf)_6(OTf)_2Sm(THF)_{10}]$, (**2**) (Scheme 1). The formation of a carbonate dianion from CO_2 with samarium complexes has precedent in the literature and several mechanisms are proposed: (i) oxo formation from CO_2 with CO release and subsequent CO_2 insertion, or (ii) reductive disproportionation of two CO_2 molecules with CO release. The key point here is that clean CO_2 in a rigorous experimental setup does not react with $Sm^{II}(OTf)_2(dme)_2$. This means that CO_2 is not the only reactant in this reaction and that the oxo intermediate mechanism should be favoured. Therefore, we started to investigate the formation mechanism of this tetrameric assembly using N_2O but also O_2 as a more challenging way of forming oxo compounds with divalent lanthanide complexes.

Reacting a degassed deep purple THF solution of $Sm(OTf)_2(dme)_2$ with N_2O leads to the complete discoloration of the solution in approximately 15 hours and an intractable white precipitate crashes out. Filtration and slow evaporation of the solvents allowed for the crystallization of the bis-oxo tetramer $[Sm_4(\mu_3\text{-}O)_2(\mu_2\text{-}OTf)_6(\mu_3\text{-}OTf)_2(THF)_4(dme)_2]$ (**1**) in good yields (85%) and in a pure analytical form. On the other hand, the reaction of $Sm(OTf)_2(dme)_2$ with one atmosphere of dry O_2 in THF is not clean and leads to an intractable clear powder and trivalent samarium triflate.

X-Ray suitable crystals of **1** were grown *via* slow diffusion of pentane in a THF solution, giving access to the topology of the oxo complex (Fig. 1A). It crystallizes in the monoclinic $P2_1/n$ space group (Table S1†). The $[Sm_2(\mu_3\text{-}O)]_2$ core of the tetramer is composed of four samarium centers bridged by two μ^3-oxo anions (Fig. 1A). In the asymmetric unit (half of the molecule) one samarium center is 8-coordinated and bears only one coordinated THF molecule, while the second one is 8-coordinated and bears one coordinated THF molecule and one dme molecule. The Sm–O distances on the O^{2-} centers are

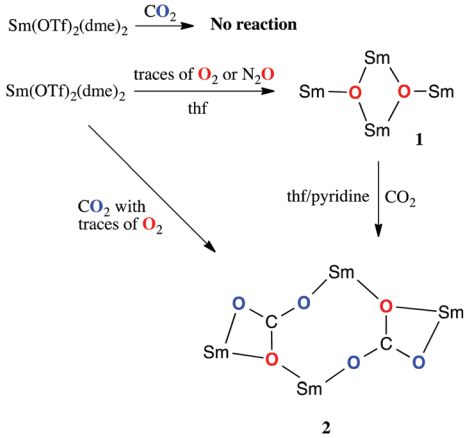

Scheme 1 Synthetic scheme for **1** and **2**.

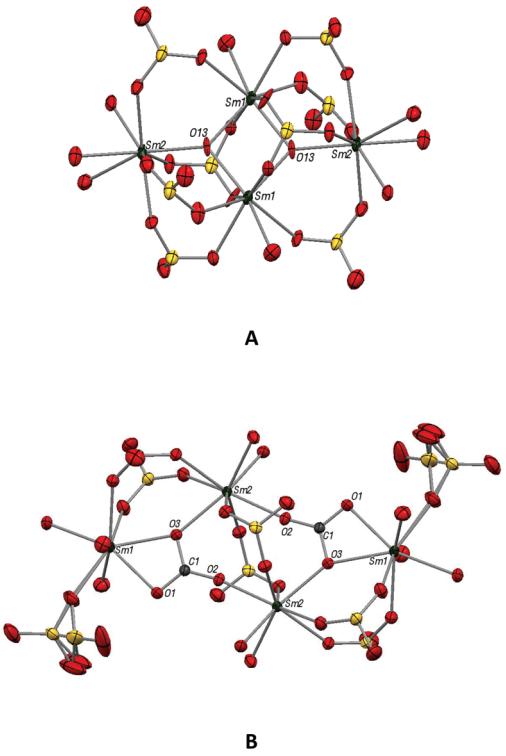

Fig. 1 (A) ORTEP of **1**; hydrogen, carbon and fluorine atoms are removed for clarity; Sm is green, O is red and S is yellow. Selected distances (Å) and angles (°): Sm01–O13 2.271(7), Sm02–O13 2.207(7), Sm01–O13#3 2.250(8), Sm01–SM01#3 3.497(1), Sm01–SM02#3 3.940 (1), Sm01–O13–Sm02 133.2(4), Sm01–O13–Sm01#3 101.3(3) and Sm01#3–O13–Sm01 124.2(3). (B) ORTEP of **2-THF**; hydrogen, carbon (except for C1) and fluorine atoms are removed for clarity; Sm is green, O is red and S is yellow. Selected distances (Å) and angles (°): Sm1–Sm2 4.580, Sm1–Sm1#2 10.102, Sm2–Sm2#2 4.522, Sm1–O1 2.379(2), Sm1–O3 2.392(2), Sm2–O2#2 2.295(2), Sm2–O3 2.362(2), O1–C1–O2 125.1(2) and O1–C1–O3 115.8(2).

2.207(7) Å, 2.258(8) Å and 2.271(7) Å, which are much longer than the Sm–O distances previously reported for μ_2-oxo (2.094 Å for the $(Cp^*_2Sm)_2(\mu\text{-}O)$ complex).[7] However, these are similar to the Sm–O distances observed for the μ_3-oxo samarium cluster (which has an average distance of 2.211 Å) reported by Hosmane.[35] The Sm–O–Sm angles (varying between 101.3(3)° and 133.2(4)°) show an important dissymmetry around the oxo where the Sm–O–Sm angles in Hosmane's cluster are between 118.9(2)° and 119.4(2)°. As expected, the triflate anions favor the tetrametallic assembly by bridging between different lanthanide centres (two of them bridge between two Sm centers whereas the third OTf^- anion of the asymmetric unit bridges between three centres). The Sm–O distances vary between 2.400(8) Å and 2.490(8) Å for μ_2-OTf^- and between 2.484(7) Å and 2.596(7) Å for μ_3-OTf^- with an average of 2.47(5) Å. These distances are shorter than the ones observed for the previously reported divalent $Sm(OTf)_2$ complexes[36] (which showed an average of 2.543 Å for $[Sm(OTf)_2(THF)_{1.5}]_n$), which is in agreement with the oxidation of the samarium center. The mean Sm–O distance is longer for

the μ_3- OTf^- anion than it is for the μ_2- OTf^- ones (2.52(7) Å *vs.* 2.45(3) Å).

Reacting a THF suspension or a THF/pyridine solution of **1** with CO_2 leads, after filtration and layering with pentane, to $[Sm_4(\mu_3\text{-}CO_3\text{-}\kappa_4O,O',O'')_2(\mu_2\text{-}OTf)_6(OTf)_2Sm(THF)_{10}]$ (**2-THF**) and $[Sm_4(\mu_3\text{-}CO_3\text{-}\kappa_4O,O',O'')_2(\mu_2\text{-}OTf)_6(OTf)_2Sm(py)_{10}]$ (**2-py**), respectively, as large colorless crystals (Fig. 1B). The **2-THF** cluster can also be obtained in good yield (80%) *via* direct reaction of the raw suspension obtained from the reaction of Sm $(OTf)_2(dme)_2$ with N_2O.

X-Ray diffraction analysis shows that **2-THF** crystallizes in a $P\bar{1}$ triclinic space-group and **2-py** does so in a $P2_1/n$ monoclinic one. For both assemblies, half the molecule is obtained as the image of the other half *via* an inversion centre and the roughly planar core can be described as $[Sm_2(\mu_3\text{-}\eta_2(O,O'):\eta_1(O):\eta_1(O')\text{-}CO_3)]_2$ with four 8-coordinate Sm surrounding two bridging carbonate anions. The carbonate coordination mode is rather unusual but has already been observed with only a few lanthanide clusters, mainly the Dy cluster, and some of them have been obtained *via* atmospheric fixation of CO_2 in aqueous media, often implying poor control of the geometry of the cluster and a long synthetic procedure.[37–40] The C–O distances in the CO_3^{2-} bridges are between 1.263(2) Å and 1.315(2) Å for **2-THF**and 1.264(8) Å and 1.301(8) Å for **2-py**, which are in the same range as the C–O distances in $NaCO_3$ (1.29 Å).[41] Here, the asymmetric coordination mode causes a strong variation between the longest C–O bonds (the oxygen bridging between two of the Sm centers) and the shortest bonds. This leads to the same disparity of bonding as the one observed by Gardiner in his porphyrinogen samarium carbonate complex (1.317(7) and 1.276(4) Å)[28] and the one observed on the $[Cp^{tt}_2Sm]_2(\mu\text{-}CO_3)$ complex (between 1.15(1) and 1.18(1) Å).[30] The carbonate Sm–O distances are similar in both **2-THF** and **2-py** with a relatively short Sm–O distance on the terminally coordinated oxygen (2.295(1) Å in **2-THF** and 2.275(5) Å in **2-py**) while the other distances are longer (between 2.373(4) and 2.399(4) Å for **2-THF** and between 2.39(1) and 2.41(1) Å for **2-py**). As for **1**, two types of triflate anion are observed, a terminal triflate ion and μ^2 bridging ones. The Sm–O distances on μ_2-TfO^- are in the same range as the ones in **1** (2.410(2) Å to 2.472(1) Å with an average of 2.45(3) Å for **2-THF** and 2.425(5) to 2.501(5) with an average of 2.46(3) Å for **2-py**). The number of coordinated solvent molecules is also identical in **2-THF** and **2-py** with two molecules on one samarium and three on the other samarium.

In solution, coordinated solvent molecules and triflate ligands are known to possibly exchange.[33] Therefore, the concentration of the THF solution of $Sm(OTf)_2(dme)_2$ strongly influences the topology of the re-crystalized species, and possibly that of the reactive species. Indeed, from a strongly concentrated solution, only the reported polymer of $[Sm(OTf)_2(THF)_{1.5}]_n$ can be recrystallized,[36] but from a diluted solution (*ca.* 10 mmol L^{-1}), a tetrametallic assembly can also be isolated (Fig. S16, Table S5†). The assembly, $[Sm_2(\mu_3\text{-}OTf)_2(\mu_3\text{-}OTf)(OTf)(THF)_6]_2$ (**3**), features relatively long Sm–O distances for the OTf^- anions (with an average of 2.63(8) Å) compared to a distance of 2.54 Å for $[Sm(OTf)_2(THF)_{1.5}]_n$.[36] Although the ^{19}F solution NMR of $Sm(OTf)_2(dme)_2$ shows only one broad signal at δ = −70.33 ppm, indicating strong exchange, the isolation of **3** as a tetrameric assembly gives an insight into the mechanism involved in the formation of **1**: the topology of the assembly may be formed prior to the reactivity with N_2O and/or it may lead to the formation of **1** by a concerted mechanism. Moreover the strong similarity between **2-THF** and **2-py** is also good evidence that the core of the cluster, once formed, can be retained in solution and that only solvent molecules exchange in the solution phase. In order to obtain better insight into the dynamics in solution, **2-THF** was recrystallized from a pyridine solution yielding **2-py**, while the fate of the triflate anions in **1** and **2** was monitored using ^{19}F NMR. For **1**, only one broad signal was observed at δ = −79.43 ppm in THF (Fig. S1†), indicating a fast exchange between the two bridging modes of the triflates. On the other hand, for **2-THF**, two broad signals were observed in the ^{19}F NMR spectrum in THF (Fig. S2†) at δ = −79.20 ppm and δ = −80.19 ppm. These two signals should correspond to the two available coordination modes of the triflate anions. The range of chemical shifts observed for both **1** and **2-THF** are close to the chemical shifts observed for $Sm(OTf)_3$ in THF (δ = −79.30 ppm and δ = −80.10 ppm) but are strongly shifted from the values of the $Sm(OTf)_2(dme)_2$ starting material, which is in agreement with the triflate anions being on the Sm^{III} centres.

The formation of **2** from **1** validates the oxo intermediate mechanism and is not surprising considering the recent studies by Roesky[42,43] and the seminal study of Meyer on uranium bridged oxo complexes.[44–46] The reaction of dry air on **1** is not clean but leads to the re-crystallization of **2**, which is indicative of selective CO_2 abstraction from air. However, the presence of humidity in air complicates the reactivity, yielding mostly $Sm(OTf)_3$. Such a selective atmospheric fixation of CO_2 on lanthanide hydroxo complexes has already been described by Mazzanti.[47]

Theoretical calculations have been performed on the formation of **1** and **2**. The addition of O_2 between two samarium centers is very favorable, in good agreement with our previous work. The key point here is that the flexibility and low steric bulk of the triflate anions allow for the addition of two more divalent samarium centers to cleave O_2 and form the bis-oxo tetrameric samarium complex **1**. As shown in Fig. 2, **1** lies −170.7 kcal mol^{-1} below the starting materials, which explains its easy formation. The CO_2 insertion on the bis-oxo complex **1** has been computed and it is indicated that the transition state is at only 11.8 kcal mol^{-1} while the reaction is exergonic by 19 kcal mol^{-1} (Fig. 2). At the transition state, the CO_2 molecule is strongly activated by two samarium atoms (the O–C–O angle is around 157°), *i.e.* a double nucleophilic assistance occurs (Sm_1–O_1: 2.60 Å, Sm_2–O_1: 2.55 Å). The oxo group O_1 adopts a pyramidal shape and lies 0.58 Å above the Sm_1–Sm_2–Sm_3 plane (compared to 0.25 Å above in complex **1**). This situation is due to the μ_3-coordination mode of the oxo O_1 that causes its remaining p lone pair to point out of the plane, inducing an out-of-plane attack of CO_2.

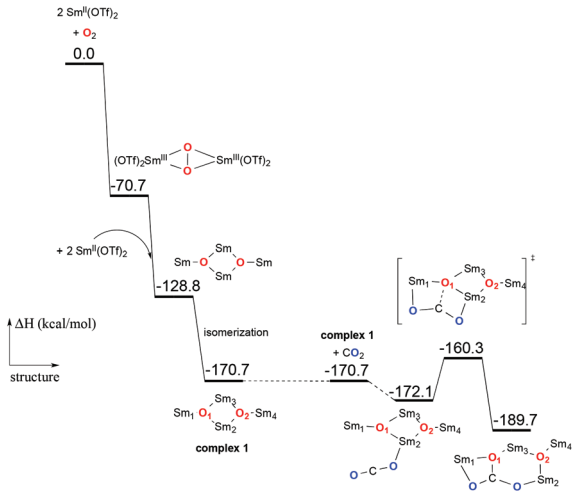

Fig. 2 Computed enthalpy profile for the O_2 reductive cleavage by four $Sm(OTf)_2$ to form **1** and the subsequent reaction with CO_2.

Since the reaction of 1 atmosphere of dry O_2 with the $Sm^{II}(OTf)_2(dme)_2$ complex in THF was not conclusive, a low amount of O_2 was used to mimic what may happen when using a lower quality CO_2 sample (*i.e.* one that contains trace amounts of O_2). The result was that the deep purple THF solution faded slowly and storage of the colorless solution at −35 °C afforded few crystals of **1** (the yield could not be calculated). The ^{19}F NMR spectrum shows the formation of a broad signal at δ = −79.81 ppm, characteristic of **1**. This indicates that the presence of traces of O_2 allows for the formation of the bis-oxo species from the synergistic actions of the four samarium centers, each providing one electron to cleave the O_2. In this example, the low bulk and the dynamics in solution of the triflate anions allow this synergy to occur. This opens new possibilities for small molecule activation with divalent lanthanides, in the opposite way to the typical strategy, which consists of increasing the steric bulk for a better stabilization of the divalent lanthanide center. This example also acts as a warning with regards to the quality of the CO_2 and the rigor of the experimental protocol that should be used for these small activation mechanistic studies.

In conclusion, this article reports the reaction of N_2O and O_2 with the $Sm(OTf)_2(dme)_2$ divalent samarium precursor to yield a rare tetrametallic bis-oxo complex of Sm^{III}. The reaction with O_2 is, to our knowledge, a unique example of the synergistic four electron reductive cleavage of O_2 with divalent lanthanide complexes. The subsequent reaction of CO_2 on this bis-oxo complex yields the tetrameric bis-carbonate samarium complex from CO_2 insertion into the oxo-bridge. This work shows that the use of less bulky divalent lanthanide complexes opens new routes for small molecule activation using the synergistic effort of multiple metal centers to cleave molecules that need more than $2e^-$, such as O_2, CO or N_2. Further studies will be conducted in this direction.

Conflicts of interest

There are no conflicts to declare.

Acknowledgements

This project was financed by the French National Agency with grant number ANR-15-CE29-0019. We thank CNRS and Ecole polytechnique for their funding. MX is grateful to the DGA for its funding. LM is a member of the Institut Universitaire de France.

Notes and references

1 C. E. Laplaza, M. J. A. Johnson, J. C. Peters, A. L. Odom, E. Kim, C. C. Cummins, G. N. George and I. J. Pickering, *J. Am. Chem. Soc.*, 1996, **118**, 8623–8638.
2 M. W. Kanan and D. G. Nocera, *Science*, 2008, **321**, 1072–1075.
3 W. Zhang, W. Lai and R. Cao, *Chem. Rev.*, 2017, **117**, 3717–3797.
4 F. Jaroschik, A. Momin, F. Nief, X. F. Le Goff, G. B. Deacon and P. C. Junk, *Angew. Chem., Int. Ed.*, 2009, **48**, 1117–1121.
5 H. B. Kagan, *J. Alloys Compd.*, 2006, **408**, 421–426.
6 M. Szostak and D. J. Procter, *Angew. Chem., Int. Ed.*, 2012, **51**, 9238–9256.
7 W. J. Evans, J. W. Grate, I. Bloom, W. E. Hunter and J. L. Atwood, *J. Am. Chem. Soc.*, 1985, **107**, 405–409.
8 C. L. Ford, Y. J. Park, E. M. Matson, Z. Gordon and A. R. Fout, *Science*, 2016, **354**, 741–743.
9 W. J. Evans, J. W. Grate and R. J. Doedens, *J. Am. Chem. Soc.*, 1985, **107**, 1671–1679.
10 W. J. Evans, M. J. Lipp, C. S. Yoo, H. Cynn, J. L. Herberg, R. S. Maxwell and M. F. Nicol, *Chem. Mater.*, 2006, **18**, 2520–2531.
11 W. J. Evans, C. A. Seibel and J. W. Ziller, *Inorg. Chem.*, 1998, **37**, 770–776.
12 A. R. Fox, S. C. Bart, K. Meyer and C. C. Cummins, *Nature*, 2008, **455**, 341–349.
13 M. Falcone, L. Chatelain, R. Scopelliti, I. Živković and M. Mazzanti, *Nature*, 2017, **547**, 332.
14 M. Falcone, C. E. Kefalidis, R. Scopelliti, L. Maron and M. Mazzanti, *Angew. Chem., Int. Ed.*, 2016, **55**, 12290–12294.
15 C. E. Laplaza and C. C. Cummins, *Science*, 1995, **268**, 861–863.
16 M. M. Rodriguez, E. Bill, W. W. Brennessel and P. L. Holland, *Science*, 2011, **334**, 780–783.
17 D. J. Knobloch, E. Lobkovsky and P. J. Chirik, *Nat. Chem.*, 2009, **2**, 30.
18 H. B. Kagan, *Tetrahedron*, 2003, **59**, 10351–10372.
19 W. J. Evans, D. S. Lee, D. B. Rego, J. M. Perotti, S. A. Kozimor, E. K. Moore and J. W. Ziller, *J. Am. Chem. Soc.*, 2004, **126**, 14574–14582.

20 F. Nief, *Dalton Trans.*, 2010, **39**, 6589–6598.
21 J. A. Bogart, C. A. Lippincott, P. J. Carroll, C. H. Booth and E. J. Schelter, *Chem. – Eur. J.*, 2015, **21**, 17850–17859.
22 J. R. Levin, T. Cheisson, P. J. Carroll and E. J. Schelter, *Dalton Trans.*, 2016, **45**, 15249–15258.
23 L. A. Solola, A. V. Zabula, W. L. Dorfner, B. C. Manor, P. J. Carroll and E. J. Schelter, *J. Am. Chem. Soc.*, 2016, **138**, 6928–6931.
24 J. A. Bogart, A. J. Lewis, S. A. Medling, N. A. Piro, P. J. Carroll, C. H. Booth and E. J. Schelter, *Inorg. Chem.*, 2013, **52**, 11600–11607.
25 G. Nocton, W. L. Lukens, C. H. Booth, S. S. Rozenel, S. A. Melding, L. Maron and R. A. Andersen, *J. Am. Chem. Soc.*, 2014, **136**, 8626–8641.
26 G. Nocton and L. Ricard, *Chem. Commun.*, 2015, **51**, 3578–3581.
27 W. J. Evans, *J. Alloys Compd.*, 2009, **488**, 493–510.
28 N. W. Davies, A. S. P. Frey, M. G. Gardiner and J. Wang, *Chem. Commun.*, 2006, 4853–4855.
29 J. Andrez, J. Pécaut, P.-A. Bayle and M. Mazzanti, *Angew. Chem., Int. Ed.*, 2014, **53**, 10448–10452.
30 M. Xémard, V. Goudy, A. Braun, M. Tricoire, M. Cordier, L. Ricard, L. Castro, E. Louyriac, C. E. Kefalidis, C. Clavaguéra, L. Maron and G. Nocton, *Organometallics*, 2017, **36**, 4660–4668.
31 L. Castro, S. Labouille, D. R. Kindra, J. W. Ziller, F. Nief, W. J. Evans and L. Maron, *Chem. – Eur. J.*, 2012, **18**, 7886–7895.
32 M. Xémard, A. Jaoul, M. Cordier, F. Molton, O. Cador, B. Le Guennic, C. Duboc, O. Maury, C. Clavaguéra and G. Nocton, *Angew. Chem., Int. Ed.*, 2017, **56**, 4266–4271.
33 G. Nocton, F. Burdet, J. Pecaut and M. Mazzanti, *Angew. Chem., Int. Ed.*, 2007, **46**, 7574–7578.
34 E. Prasad, B. W. Knettle and R. A. Flowers, *J. Am. Chem. Soc.*, 2002, **124**, 14663–14667.
35 N. S. Hosmane, Y. Wang, A. R. Oki, H. Zhang and J. A. Maguire, *Organometallics*, 1996, **15**, 626–638.
36 K. Mashima, T. Oshiki and K. Tani, *J. Org. Chem.*, 1998, **63**, 7114–7116.
37 A. S. R. Chesman, D. R. Turner, B. Moubaraki, K. S. Murray, G. B. Deacon and S. R. Batten, *Dalton Trans.*, 2012, **41**, 10903–10909.
38 I. A. Gass, B. Moubaraki, S. K. Langley, S. R. Batten and K. S. Murray, *Chem. Commun.*, 2012, **48**, 2089–2091.
39 L.-L. Li, R. Pan, J.-W. Zhao, B.-F. Yang and G.-Y. Yang, *Dalton Trans.*, 2016, **45**, 11958–11967.
40 S. Xue, L. Zhao, Y.-N. Guo, P. Zhang and J. Tang, *Chem. Commun.*, 2012, **48**, 8946–8948.
41 M. Dusek, G. Chapuis, M. Meyer and V. Petricek, *Acta Crystallogr., Sect. B: Struct. Sci.*, 2003, **59**, 337–352.
42 C. Schoo, S. V. Klementyeva, M. T. Gamer, S. N. Konchenko and P. W. Roesky, *Chem. Commun.*, 2016, **52**, 6654–6657.
43 E. Louyriac, P. W. Roesky and L. Maron, *Dalton Trans.*, 2017, **46**, 7660–7663.
44 O. P. Lam, S. M. Franke, F. W. Heinemann and K. Meyer, *J. Am. Chem. Soc.*, 2012, **134**, 16877–16881.
45 A. C. Schmidt, F. W. Heinemann, C. E. Kefalidis, L. Maron, P. W. Roesky and K. Meyer, *Chem. – Eur. J.*, 2014, **20**, 13501–13506.
46 O. P. Lam, S. C. Bart, H. Kameo, F. W. Heinemann and K. Meyer, *Chem. Commun.*, 2010, **46**, 3137–3139.
47 L. Natrajan, J. Pecaut and M. Mazzanti, *Dalton Trans.*, 2006, 1002–1005.

